Photo-neutron cross-section of ^{100}Mo

Rita Crasta · H. Naik · S. V. Suryanarayana ·
P. M. Prajapati · K. C. Jagadisan · S. V. Thakare ·
S. Ganesh · V. T. Nimje · K. C. Mittal · A. Goswami

Abstract The ^{100}Mo(γ, n) reaction cross-section was experimentally determined at end point bremsstrahlung energy of 10 and 12.5 MeV using off-line γ-ray spectrometric technique. It was also found that ^{100}Mo(γ, n) reaction cross-section increases sharply from the end point bremsstrahlung energy of 10 MeV to 12.5 MeV, which may be because of GDR around the energy region of 12–16 MeV. The ^{100}Mo(γ, n) reaction cross-section as a function of photon energy was calculated theoretically using TALYS 1.2 computer code. The flux-weighted average values of ^{100}Mo(γ, n) reaction cross-section for bremsstrahlung having end point energy of 10 and 12.5 MeV were also calculated using the experimental and theoretical data of mono-energetic photon. The present experimental ^{100}Mo(γ, n) reaction cross-sections were compared with the bremsstrahlung flux-weighted average values of experimental and theoretical data and found to be in the lower side for 10 MeV and in the higher side for 12.5 MeV.

R. Crasta · S. Ganesh
Department of Studies in Physics, Microtron Centre, Mangalore University, Mangalagangotri 574 199, Karnataka, India

H. Naik (✉) · A. Goswami
Radiochemistry Division, Bhabha Atomic Research Centre, Mumbai 400085, India
e-mail: naikhbarc@yahoo.com

S. V. Suryanarayana
Nuclear Physics Division, Bhabha Atomic Research Centre, Mumbai 400085, India

P. M. Prajapati
Reactor Physics Design Division, Bhabha Atomic Research Centre, Mumbai 400085, India

K. C. Jagadisan · S. V. Thakare
Radio Pharmaceutical Division, Bhabha Atomic Research Centre, Mumbai 400085, India

V. T. Nimje · K. C. Mittal
Accelerator & Pulse Power Division, Bhabha Atomic Research Centre, Mumbai 400085, India

Introduction

Radioactive isotopes are widely used in industry, medicine and the life sciences [1]. Among 3,000 isotopes, approximately 140 radioisotopes are used worldwide in medical application such as diagnostic, therapeutic and preventive purpose. The use of medical radioisotopes is an important part of modern medical practices. Medical isotopes are used in non-invasive nuclear diagnostic imaging techniques to help, identify common illnesses such as heart diseases and cancer at an early stage [2–6]. Out of the 140 radioisotopes only ten isotopes are used in 90% of all in vivo nuclear medicine procedures performed per year [7, 8]. The most widely used medical radioisotope, ^{99m}Tc, is essential for an estimated 70,000 medical imaging procedures that take place daily around the world. ^{99m}Tc is a medical isotope, utilized in over 80% of all nuclear medicine studies [9–11]. ^{99m}Tc is a critical medical isotope used in diagnostic and functional studies or organs and anatomical systems. It is used primarily to locate tumors in the body, monitor cardiac function following heart attacks, map blood flow in the brain and guide surgery. The information from these studies is used by many medical

specialists including radiologists, cardiologists, nephrologists and oncologists to better diagnose and treat patients. It is also used for brain, cerebral perfusion, liver, bone and bone marrow, blood pool, and pulmonary perfusion imaging etc., [12, 13]. More than 30 million nuclear medicine procedures are performed worldwide each year using ^{99m}Tc. ^{99m}Tc having half-life of 6 h that decays to the much longer lived ^{99g}Tc by emitting a 140.5 keV γ-ray. It can be bound into a variety of special molecules that target specific parts of the body when ingested or injected [14, 15]. By detecting the 140.5 keV γ-rays its location within the body can be pinpointed. Because of the several applications in the areas of diagnostic nuclear medicine, radionuclide ^{99m}Tc plays an important role [12, 13].

Usually ^{99m}Tc is produced by milking out from the parent ^{99}Mo having half-life of 65.94 h [16–18]. Natural Mo is an important material and is used as a target material for the production of medical radio isotopes like as ^{99}Mo-^{99m}Tc, ^{96}Tc, ^{94m}Tc etc., by using different nuclear reactions. In principle the radionuclide ^{99}Mo can be produced in various ways. In every day practice ^{99}Mo is produced almost 100% by use of research reactors. Currently, the dominant route is the neutron induced fission of enriched ^{235}U through the reaction ^{235}U(n, f) ^{99}Mo and by the neutron capture through the reaction ^{98}Mo(n, γ) ^{99}Mo, which transmute a stable isotope into a radioactive isotope of the same element. High specific activities are obtained, when the ^{98}Mo(n, γ) ^{99}Mo cross-section is high and the target is irradiated with a high neutron flux density. In neutron induced fission of ^{235}U many long-lived radioactive wastes with total activity of fifty times the activity of ^{99}Mo are formed [19–21]. Proton accelerators in terms of MeV region designed for medical radio-nuclides productions are available and already in use over the world. The proton induced nuclear reactions on natural molybdenum containing ^{92,94,95,96,97,98,100}Mo isotopes can also form many radioactive products with high activities. It is possible to make production of ^{99m}Tc and ^{99}Mo by the proton bombardment [22–24] via the most suitable reactions ^{100}Mo(p, pn) ^{99m}Tc and ^{100}Mo(n, 2n) ^{99}Mo, respectively. ^{99}Mo-^{99m}Tc can also be obtained by the ^{100}Mo(γ, n) ^{99}Mo photo-nuclear reaction [25–27] on an electron accelerator.

Cross-section measurements for nuclear photo disintegration have been under taken in recent years by use of several sources of γ-rays [27–30]. Owing to the development of accelerator technology, the performance and the reliability of accelerators were improved in recent years. Thereby, the use of the accelerators is extended to material studies, medical treatment, radiobiological studies and environmental science. Now a day's most photo-nuclear studies have been made by use of electron bremsstrahlung produced by electron accelerators. However, the bremsstrahlung is continuous in distribution up to the energy of the electrons and has its greatest intensity at low energies.

Activation cross-section data are also required for radiation safety, calculations of absorbed dose in the human body during radiotherapy and estimation of radioactive wastes [31]. Therefore, the activation cross-section of Mo for photon beam is required over a wide energy range. Very few experimental works on mono-energetic photon induced reaction cross-section measurement of ^{100}Mo(γ, n) at different energies is available in the literature [32, 33] using activation technique. In their study [32] mono-chromatic photon beam is used to find the reaction cross-section. Production of sufficiently useable activity of ^{99}Mo from ^{100}Mo(γ, n) reaction with mono-energetic photon is a difficult task. This is because in electron linac, the photon energy available is not mono-energetic but in the form of bremsstrahlung radiation. Thus, it is worth to examine the ^{100}Mo(γ, n) cross-section with bremsstrahlung radiation instead of mono-energetic photon. In literature, there is no data on ^{100}Mo(γ, n) cross-section are available on bremsstrahlung induced reaction. In view of this, in the present study we have measured the reaction cross-section for the ^{100}Mo(γ, n) reactions at end point bremsstrahlung energy of 10 and 12.5 MeV using activation followed by off-line γ-ray spectrometry technique. The ^{100}Mo(γ, n) reaction cross-section induced by 10 and 12.5 MeV bremsstrahlung was also calculated theoretically using a TALYS 1.2 code [34] and the result was compared with experimental value of the present study.

Experimental procedure

The experiments were performed by using the bremsstrahlung beams with end point energies of 10 and 12.5 MeV, in the electron LINAC of the electron beam centre (EBC) at Kharghar, Navi-Mumbai, India. The photons beam was produced when the pulsed electrons of 10 MeV hit a thick tantalum metal foil having a thickness of 1 mm placed at a distance of 10 cm on a suitable stand facing the electron beam aperture. In case of 12.5 MeV electron beam, a thin Ta foil of 0.25 mm thick was used to avoid neutron production.

Two sets of high purity ^{nat}Mo and ^{nat}Au metal target foils were separately wrapped with 0.025 mm thick super pure aluminum foil. Each set of ^{nat}Mo and ^{nat}Au sample wrapped with Al foil were covered with additional Al foil of same thickness. The ^{nat}Au foil was used as monitor for the determination of bremsstrahlung flux. In the first set for end point bremsstrahlung energy of 10 MeV, the weight of ^{nat}Mo and ^{nat}Au were 0.1191 and 0.05435 g, respectively. Similarly for the second set for end point bremsstrahlung energy of 12.5 MeV, the weight of ^{nat}Mo and ^{nat}Au were 0.0172 and 0.0556 g, respectively. These sets of samples were placed in air below the tantalum foil for individual
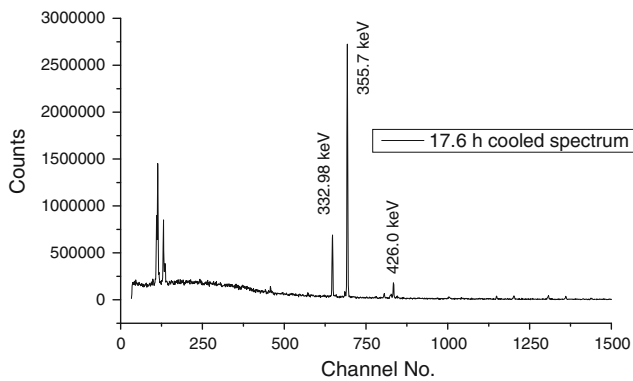
Fig. 1 Typical γ-ray spectrum of an irradiated gold foil showing the γ-lines of ^{196}Au
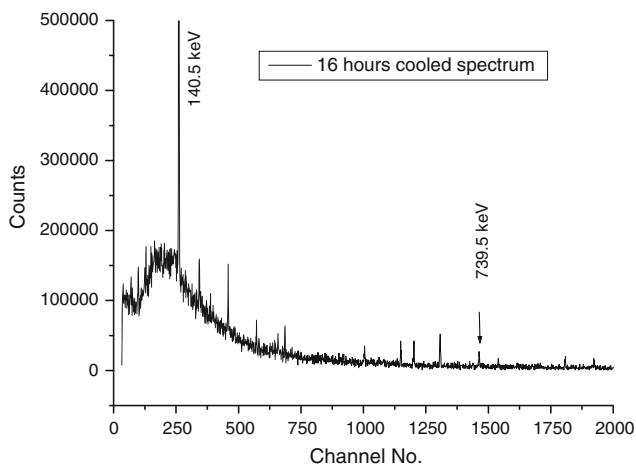
Fig. 2 Typical γ-ray spectrum of an irradiated ^{100}Mo showing the γ-lines of ^{99}Mo

irradiation. The samples were irradiated one after another for 2–3 h with the end point bremsstrahlung energy of 10 and 12.5 MeV, respectively. During the irradiation, the electron linac was operated with a pulse repetition rate of 400 and 310 Hz, pulse width of 10 μs and the average beam current of 50 and 25 mA for 10 and 12.5 MeV, respectively. After 2–3 h cooling time, the Al cover of the irradiated targets was removed. Then the irradiated targets of Mo and Au along with aluminum wrapper were mounted on different Perspex plates and taken for γ-ray counting.

The γ-ray activities of the foils were measured using an energy- and efficiency-calibrated 80 cc HPGe detector, coupled to a PC based 4 K channel analyzer. The energy resolution of the detector system was 2.0 keV at 1332.0 keV of ^{60}Co. The dead time of the detector system during counting was always kept as less than 10% by placing the sample at a suitable distance from the detector to avoid the pile up effect. The γ-ray counting of the sample was done in live time mode and was followed by a function of time. Typical γ-ray spectrum of irradiated ^{nat}Au and ^{nat}Mo are given in Figs. 1 and 2, respectively.

Calculations and results

Calculation of the photon flux

The photo-peak areas of different γ-rays of nuclides of interest were calculated by subtracting the linear Compton background from their net peak areas. The photon flux was determined based on the activity of 355.7 keV γ-line from ^{197}Au(γ, n) ^{196}Au reaction [35, 36]. Photon flux and the photo-peak activities (A_{obs}) for 355.7 keV γ-line of ^{196}Au nuclide are related by the equation,

$$A_{(obs)}(CL/LT) = N <\sigma> \varphi a\varepsilon(1 - e^{-\lambda t})e^{-\lambda T} \times (1 - e^{-\lambda CL})/\lambda \tag{1}$$

where N is the number of target atoms. $<\sigma>$ is the average cross-section of ^{197}Au(γ, n) ^{196}Au reaction, which was taken from Ref. [37]. 'a' is the branching intensity and ε is detection efficiency for the 355.7 keV γ-lines of the ^{196}Au. 't' and T are the irradiation and cooling times whereas, CL and LT are the clock time and live time of counting, respectively. In the above equation the CL/LT term has been used for dead time correction. The γ-ray energies and the nuclear spectroscopic data such as the half-lives and branching ratios of the reaction products are taken from Refs. [16, 17, 38] and given in Table 1.

The average cross-section ($<\sigma>$) for ^{197}Au(γ, n) ^{196}Au reaction was calculated using the relation

$$<\sigma> = \Sigma(\sigma\varphi)/\Sigma\varphi \tag{2}$$

where φ is photon flux for ^{197}Au(γ, n) reaction. The photon flux (φ) as a function of photon energy was calculated by using EGS4 code [39], which is shown in Fig. 3. For a particular energy E, the $<\sigma>$ was obtained from evaluated data [37] of mono-energetic photon as well as from theoretical value based on TALYS 1.2 [34] computer code (Fig. 4), which is described in the next section. The flux-weighted average σ values for ^{197}Au(γ, n) reaction from evaluated and theoretical data are shown in Table 2. Then the photon flux for ^{197}Au(γ, n) reaction was calculated using the equation given below,

$$\varphi = A_{obs}(CL/CT)\lambda/N <\sigma> a\varepsilon(1 - e^{-\lambda t})e^{-\lambda T} \times (1 - e^{-\lambda CL}). \tag{3}$$

The reaction threshold for ^{197}Au(γ, n) is 8.0725 MeV and that for ^{100}Mo(γ, n) reaction is 8.2901 MeV. Thus for 10 MeV bremsstrahlung the weighted average flux obtained from ^{197}Au(γ, n) reaction is multiplied by 0.83, which is the flux ratio of ^{100}Mo(γ, n) reaction from 8.29 to 10 MeV to the ^{197}Au(γ, n) reaction from 8.07 to 10 MeV bremsstrahlung energy. Similarly for 12.5 MeV bremsstrahlung, the weighted average flux obtained from

Table 1 Nuclear spectroscopic data used in the calculation

Nuclide	Half-life	γ-Ray energy (keV)	γ-Ray abundance (%)	References
[196]Au	6.183 days	332.983	22.9	[16, 17, 38]
		355.689	87	
		426.0	7	
[99]Mo	65.94 h	140.511	89.43	[16, 17, 40]
		739.5	12.13	
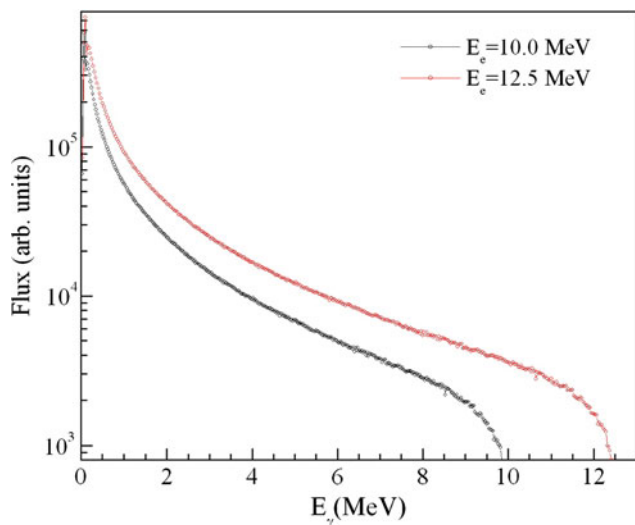
Fig. 3 Plot of bremsstrahlung spectrum for end point energy of 10 and 12.5 MeV
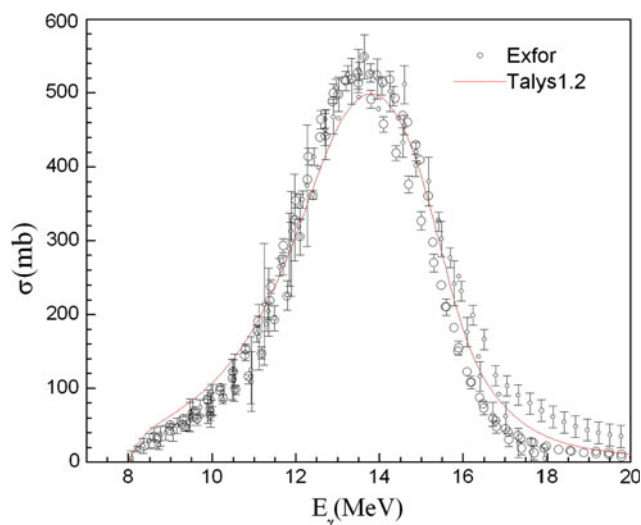
Fig. 4 Plot of experimental and theoretical [197]Au(γ, n) reaction cross-section as a function of photon energy

[197]Au(γ, n) reaction is multiplied by 0.897, which is the flux ratio of [100]Mo(γ, n) reaction from 8.29 to 12.5 MeV to the [197]Au(γ, n) reaction from 8.07 to 12.5 MeV

bremsstrahlung energy. The experimentally obtained photon flux is given in Table 2. The bremsstrahlung flux at end point energy of 10 MeV energy is higher than 12.5 MeV due to the higher beam current of 50 mA in the former compared to 25 mA in the later.

Photo-neutron cross-section for [100]Mo(γ, n) [99]Mo

The photon irradiation on [100]Mo target resulted in the production of [99]Mo radionuclide through the (γ, n) process. The decay data of the radio-active products, contributing reaction process and threshold energy are taken from the Refs. [16, 17, 40] and are presented in the Table 1. The unstable radio nuclide [99]Mo ($t_{1/2} = 65.94$ h), which is produced by the [100]Mo(γ, n) [99]Mo reaction decays to [99m]Tc ($t_{1/2} = 6.01$ h) by β^- process. The [99]Mo radionuclide was identified through an analysis of the 140.5 and 739.5 keV characteristic γ-lines (Fig. 2). The number of detected γ-rays (A_{obs}) of the reaction product [99]Mo was used to calculate the photo-neutron cross-section of [100]Mo using the Eq. 1 and is rewritten as

$$\sigma = A_{obs}(CL/CT)\lambda/N\varphi a\,\varepsilon\,(1 - e^{-\lambda t})\,e^{-\lambda T}(1 - e^{-\lambda CL}) \tag{4}$$

where φ is average flux for [100]Mo(γ, n) reaction, the rest of the terms have the similar meaning as in the Eq. 1 The photo-neutron cross-section for the [100]Mo(γ, n) [99]Mo reaction has been measured relative to the reference photo-neutron cross-section value of [197]Au(γ, n) [196]Au reaction for end point bremsstrahlung energy of 10 and 12.5 MeV, respectively.

Results and discussion

The photo-neutron cross-section of the [100]Mo(γ, n) [99]Mo reaction measured in the present work for end point bremsstrahlung energy of 10 and 12.5 MeV are determined for the first time and are given in Table 2. The uncertainties associated to the measured cross-sections come from the combination of two experimental data sets. This overall uncertainty is the quadratic sum of both statistical and systematic errors. The random error in the observed activity is primarily due to counting statistics, which is estimated to be 5–10%. This can be determined by accumulating the data for an optimum time period that depends on the half-life of nuclides of interest. The systematic errors are due to uncertainties in photon flux estimation ($\sim 4\%$), the irradiation time ($\sim 0.5\%$), the detection efficiency calibration ($\sim 3\%$), the half-life of the reaction products and the γ-ray abundances ($\sim 2\%$) as reported in the literature [16, 17, 38, 40]. Thus the total systematic error is about $\sim 5.4\%$. The overall uncertainty is found to

Table 2 ^{100}Mo(γ, n) reaction cross-section at different bremsstrahlung energies

Photon energy (MeV)	Flux-weighted ^{197}Au(γ, n) $<\sigma>$ (mb) [Ref]	Flux (φ) × 10^8 (photons/cm^2/s)	γ-Ray energy of ^{99}Mo (keV)	^{100}Mo(γ, n) σ (mb)
10	38.65 [37]	20.01 ± 0.72	140.5	10.95 ± 0.65
			739.5	9.69 ± 1.14
10	55 [34]	14.06 ± 0.51	140.5	15.57 ± 0.92
			739.5	13.72 ± 1.50
12.5	95.35 [37]	6.50 ± 0.07	140.5	76.16 ± 4.01
			739.5	54.58 ± 3.94
12.5	113.9 [34]	5.44 ± 0.06	140.5	90.94 ± 4.79
			739.5	65.17 ± 4.71

Table 3 Comparison of ^{100}Mo(γ, n) reaction cross-section obtained from the end point energy of bremsstrahlung spectrum and flux-weighted average of mono-energetic photon

| End point bremsstrahlung energy (MeV)	Experimental cross-section based on 739.5 keV γ-line (mb)	Cross-section using literature [29] (mb)	Cross-section using TALYS (mb)
10	9.7–13.7	14.15	25.67
12.5	54.6–65.4	28.27	40.03

range between 7.4 and 11.4%, coming from the combination of a statistical error of 5–10% and a systematic error of 5.4%.

It can be seen from Table 2 that at the experimentally determined ^{100}Mo(γ, n) cross-section based on 140.5 keV γ-energy increases from 11 to 15 mb at end point bremsstrahlung energy of 10 MeV to 76–91 mb at 12.5 MeV. On the other hand the experimentally determined ^{100}Mo(γ, n) cross-section based on 739.5 keV γ-energy increases from 9.7 to 13.7 mb at end point bremsstrahlung energy of 10 MeV to 55–65 mb at 12.5 MeV. Slight higher cross-section based on 140.5 keV γ-ray energy of ^{99}Mo is most probably due to the interference of same γ-line of its daughter ^{99m}Tc. The range of ^{100}Mo(γ, n) cross-section for same end point bremsstrahlung energy for both γ-energies is due to the use of two different types of photon flux based on experimental and theoretical ^{197}Au(γ, n) reaction cross-section, which were shown in Table 2.

In literature [32] the experimental data on photo-neutron cross-section of ^{100}Mo available are only mono-energetic photon. The ^{100}Mo(γ, n) reaction cross-section of literature data for mono-energetic photon [32] also increases with increase of photon energy up to 14 MeV and there after it decreases due to opening of other reaction channels. The higher photo-neutron cross-section of ^{100}Mo within the photon energy of 12–16 MeV is due to Giant Dipole Resonance (GDR) effect. Thus, higher photo-neutron

cross-section of ^{100}Mo for end point bremsstrahlung energy of 12.5 MeV from present study is also due to GDR effect. In order to examine this effect the photo-neutron cross-section of ^{100}Mo as a function of mono-energetic photon energy from literature [32] is plotted in Fig. 5. From Fig. 5 the flux-weighted ^{100}Mo(γ, n) reaction cross-sections at end point bremsstrahlung of 10 and 12.5 MeV are calculated using Eq. 2 and are given in Table 3 along with experimental data for comparison. The photon flux as function of energy was taken from Fig. 3. It can be seen from Table 3 that the ^{100}Mo(γ, n) reaction cross-section from present experiment at end point bremsstrahlung of 10 MeV is lower and it is higher at 12.5 MeV than the flux-weighted average value of literature data [32]. This is most probably due to bremsstrahlung spectrum based on EGS code [39] or may be due to GDR effect. Further to examine this aspect the ^{100}Mo(γ, n) reaction cross-section as a function of photon energy was calculated theoretically using TALYS computer code 1.2 [34].

TALYS [34] is a computer code for the prediction and analysis of nuclear reactions that involve photons, neutrons, protons, deuterons, tritons, hellions and alpha particles, in the 1 keV–200 MeV energy range and for target nuclides of masses 12 and heavier. For this, TALYS integrates the optical model, direct, pre-equilibrium, fission and statistical nuclear reaction models in one calculation scheme and thereby gives a prediction for all the open reaction channels. In TALYS, several options are included for the choice of different parameters such as γ-strength functions, nuclear level densities and nuclear model parameters etc. In the present study, we calculated photon-induced reaction cross-sections of ^{197}Au and ^{100}Mo target using the default option in the TALYS code [34]. All possible outgoing channels for the given photon energy were considered. However, the cross-section for the (γ, n) reaction was specially looked for and collected. The (γ, n) reaction cross-section as a function of photon energy for ^{197}Au and ^{100}Mo are plotted in Figs. 4 and 5, respectively. It can be seen from Figs. 4 and 5 that
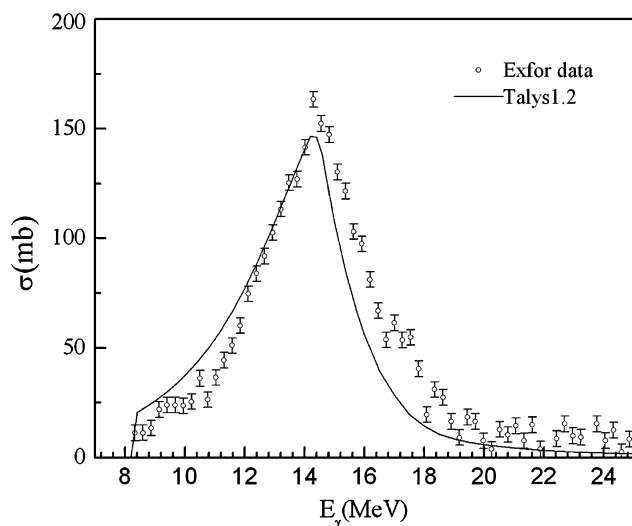
Fig. 5 Plot of experimental and theoretical ^{100}Mo(γ, n) reaction cross-section as a function of photon energy

^{197}Au(γ, n) and ^{100}Mo(γ, n) reaction cross-section as a function of photon energy from Talys 1.2 shows a similar structure as of the experimental data [34]. However, slight left side shift is there in theoretical calculated cross-section, which may be due to the use of default parameters in the TALYS calculation. From Figs. 4 and 5 theoretical flux-weighted ^{197}Au(γ, n) and ^{100}Mo(γ, n) reaction cross-section were calculated using Eq. 2. The photon flux as function of energy from the bremsstrahlung spectrum of Fig. 3 was used in the calculation. The theoretically calculated flux-weighted ^{197}Au(γ, n) reaction cross-section, which was used for flux determination is given in Table 2. On the other hand the theoretically calculated flux-weighted ^{100}Mo(γ, n) reaction cross-section is given in the last column of Table 3 to compare with experimental data.

It can seen from Table 3 that the experimentally determined ^{100}Mo(γ, n) reaction cross-section at end point bremsstrahlung energy of 10 MeV was closer to the flux-weighted value obtained from experimental mono-energetic photon data [32] and lower than the flux-weighted theoretical value. On the other hand the experimentally determined ^{100}Mo(γ, n) reaction cross-section at end point bremsstrahlung energy of 12.5 MeV was higher from flux-weighted value based on experimental mono-energetic photon data [32] and theoretical data. The experimental ^{100}Mo(γ, n) reaction cross-section as a function of end point bremsstrahlung energy will help to estimate the activity of important medical isotope ^{99}Mo-^{99m}Tc produced using electron linac. This can give idea and feasibility of ^{99}Mo-^{99m}Tc production in electron linac in the absence of nuclear reactor.

Conclusion

(i) The photo-neutron cross-section for the ^{100}Mo(γ, n) ^{99}Mo reaction at end point bremsstrahlung energy of 10 and 12.5 MeV have been determined for the first time using off-line and γ-ray spectrometric technique.

(ii) The photo-neutron cross-section of the ^{100}Mo(γ, n) ^{99}Mo reaction increases sharply from end point bremsstrahlung energy of 10 MeV to 12.5 MeV. Unusual higher cross-section at 12.5 MeV is most probably due to the Giant Dipole Resonance (GDR) effect.

(iii) The ^{100}Mo(γ, n) ^{99}Mo reaction cross-section as a function of photon energy was theoretically calculated using computer code Talys 1.2. The flux-weighted average cross-section of ^{100}Mo(γ, n) ^{99}Mo reaction was also calculated from the experimental and theoretical cross-section of mono-energetic photon and compared with the present experimental value.

(iv) The experimental ^{100}Mo(γ, n) reaction cross-section at end point bremsstrahlung energy of 10 MeV was found to be closer to the flux-weighted average experimental value but is lower than the theoretical value from mono-energetic photon data. On the other hand the experimental value at end point bremsstrahlung energy of 12.5 MeV is significantly higher than the flux-weighted average experimental and theoretical value.

References

1. Larsson CL (2004) "Availability and Use of Medical Isotopes in Canada", TM 2004-218, OMB no. 0704-0188. Defense Research and Development Canada (DRDC), Ottawa
2. Cameron CB (1970) J Clin Pathol April 23(3):280
3. Schiepers C (2006) Diagnostic nuclear medicine. Springer, Berlin
4. Royston HF, Jeremy JL, Buckeley Pal T, Daniel LD, James TE, Paulenova A (2006) J Chem Educ 83:625
5. Cook GJR (2006) Clin Nucl Med 1:5–27
6. Cook GJR (2003) Br J Radiol 76:S152–S158
7. National Council of Radiation Protection and Measurements (NCRP) (1996) Sources and magnitude of occupational and

public exposures from nuclear medicine procedures, NCRP Report No 124. NCRP, Bethesda

8. International Atomic Energy Agency (2003) Categorization of radioactive sources- Revision of IAEA-TECDOC-1191, Categorization of radioactive sources- Revision of IAEA-TECDOC-1344, IAEA, Vienna

9. Scholten B, Lambrecht RM, Michel C, Hernan VR, Qaim SM (1999) Appl Radiat Isot 51:69

10. Froment P, Tilquin I, Cogneau M, Delbar Th, Vervier J, Ryckewaert G (2002) Nucl Instrum Methods Phys Res 493:165

11. Sabel'nikov AV, Maslov OD, Molokanova LG, Gustova MV, Dmitriev SN (2006) Radiokhimiya 48:172 or Radiochemistry 48:191

12. Ruth T (2009) Nature 457:536–537. doi:10.1038/nature07540

13. IAEA (2001) Charged particle cross-section data base for medical radioisotope production:diagnostic radioisotopes and monitor reactions, IAEA-TECDOC-1211. http://www-nds.iaea.org. Accessed May 2001

14. Gambini JP, Cabral P, Alonso O, Savio E, Figueroa SD, Zhang X, Lixin M, Susan LD, Thomas PQ (2011) Nucl Med Biol 38:255

15. Terán MA, Elena M, Reyes AL, Andrea P, Marcelo V, Patricia E, Jose PP, Eduardo S (2011) Nucl Med Biol 38:279

16. Browne E, Firestone RB (1986) In: Shirley VS (ed) Table of radioactive isotopes. Wiley, New York

17. Firestone RB, Ekstrom LP (2004) Table of radioactive isotopes. Lawrence Berkeley National Laboratory, Berkeley

18. Blachot J, Fiche Ch (1981) Ann Phys 6:3–218

19. Bourges J, Madic C, Koehly G, Nguyent H, Baltes D, Landesman C, Simon A (1996) Nucl Technol 113:204

20. Richards P (965) Report no. BNL 9601. Brookhaven National Laboratory, Long Island

21. Arino H, Frank J C, Kenneth D G, Alfred K T (1976) US Patent 3,940,318, 24 February 1976

22. Uddin MS, Baba M (2008) Appl Radiat Isot 66:208

23. Uddin MS, Hagiwara M, Tarkanyi F, Ditroi F, Baba M (2004) Appl Radiat Isot 60:911

24. Krivan V (1975) Anal Chim Acta 79:161

25. Habs D, Köster U (2010) Appl Phys B. doi:10.1007/s00340-010-4261-x

26. Uvarov VL, Dikiy NP, Dovbnya AN, Medvedyeva YP, Pugachov GD, Tur YD (1997) Particle accelerator conference, Proceedings of the 1997. American Physical Society, San Antonio

27. Titus WF (1959) Phys Rev 115:351

28. Naik H, Sarbjit Singh, Goswami A, Manchanda VK, Kim G, Kim KS, Lee M, Shakilur MR, Raj D, Ganesan S, Suryanarayana SV, Cho M-H, Namkung W (2011) Nucl Inst Methods Phys Res B 269:1417

29. Kim KS, Shakilur Rahman MD, Lee M, Kim G, Khue PD, Do NG, Cho M-H, Ko IS, Namkung W, Naik H, Ro Tae Ik (2011) J Radioanal Nucl Chem 287:869

30. Thiep TD, An TT, Khai NT, Cuong PV, Vinh TN (2010) J Radioanal Nucl Chem 286:161

31. IAEA (2000) Hand book on photonuclear data for applications cross-sections and spectra. IAEA-TECDOC-1178. IAEA, Vienna. http://www-nds.iaea.org

32. Beil H, Bergere R, Carols P, Lepretre A, de Miniac A, Veyssiere A (1974) Nucl Phys A 227:427

33. Gellie RW (1968) Aust J Phys 21:765

34. Koning AJ, Hilaire S, Duijvestijn MC (2005) TALYS: comprehensive nuclear reaction modeling. In: Haight RC, Chadwick MB, Kawano T, Talou P (eds) Proceedings of the international conference on nuclear data for science and technology-ND 2004, AIP vol 769. Santa Fe, USA, pp 1154–1159

35. Yoshinaga O, Toyoaki K, Nobuyoshi S (1969) Bull Chem Soc Jpn 42:387

36. Yamadera A, Yoshitomo U, Nakamura T (1993) Nucl Instrum Methods Phys Res A329:188

37. Varlamov VV, Ishkhanov BS, Orlin VN, Yu TS (2010) Ser Fiz 74:884

38. Xiaolong H (2007) Nucl Data Sheets 108:1093

39. Nelson WR, Hirayama H, Rogers DWO (1985) SLAC-Report-265. Linear Accelerator Center, Stanford

40. Medsker LR (1974) Nucl Data Sheets 12:431